Hindawi Publishing Corporation
Journal of Solid State Physics
Volume 2013, Article ID 451563, 9 pages
http://dx.doi.org/10.1155/2013/451563

Research Article

Dielectric Properties of Rhombohedral $PbNb_2O_6$

Kriti Ranjan Sahu[1] and Udayan De[2]

[1] *Physics Department, Egra SSB College, Egra, West Bengal 721429, India*
[2] *Kendriya Vihar C-4/60, V.I.P. Road, Kolkata 700052, India*

Correspondence should be addressed to Udayan De; ude2006@gmail.com

Received 30 April 2013; Revised 26 August 2013; Accepted 20 September 2013

Academic Editor: Hamdy Doweidar

Dielectric materials are needed in many electrical and electronic applications. So, basic characterizations need to be done for all dielectrics. $PbNb_2O_6$ (PN) is ferroelectric and piezoelectric only in its orthorhombic phase, with potential high temperature applications. So, its rhombohedral phase, frequently formed as an undesirable impurity in the preparation of orthorhombic PN, has been ignored with respect to possible dielectric characterizations. Here, essentially single phase rhombohedral PN has been prepared, checking structure from XRD Rietveld Analysis, and the real and imaginary parts of permittivity measured in an Impedance Spectrometer (IS) up to ~ 700°C and over 20 Hz to 5.5 MHz range, for heating and some cooling runs. Variations, with temperature, of relaxation time constant (τ), AC and DC conductivity, bulk resistance, activation energy and capacitance have been explored from our IS data.

1. Introduction

Commercial piezoelectric (PE) materials for applications in medicine, industry, and research have mostly been barium titanate ($BaTiO_3$), lead zirconate titanate ($Pb[Zr_xTi_{1-x}]O_3$, $0 \leq x \leq 1$, or PZT), or materials based on one of these. But Curie temperature, the upper limit for piezoelectricity, is at best 130°C [1, 2] for the former and 390°C [2] for a specially modified PZT. Now, certain modern high temperature applications in industry need higher Curie temperature and, hence, newer materials with higher Curie temperature and suitable PE properties. This growing need for high temperature piezoelectric sensors and actuators [1, 2] has revived, in last few decades, a worldwide interest in lead niobate ($PbNb_2O_6$, to be shortened here as PN) in orthorhombic structure, which alone is piezoelectric. It was discovered [3] in 1953 but almost ignored for decades after a wave of pioneering work [3–5] of high quality. PN and PN-based ferroelectric samples involving chemical substitution &/or composite formation [6–8] are now being investigated by different groups, while present work is on pure $PbNb_2O_6$ in rhombohedral form.

$PbNb_2O_6$ has different structures as already indicated. The stable forms of $PbNb_2O_6$ are [3–5, 9] rhombohedral (at low temperature) and tetragonal (at high temperature). The latter is transformed, usually by quenching (*Q*), to PNQ, the metastable orthorhombic $PbNb_2O_6$, which alone can be made piezoelectric (fortunately with a high Curie temperature higher than 580°C for 5.5 MHz, e.g., [9]). Slow (*S*) cooling (from temperatures like 1270°C) leads [10, 11] to PNS, rhombohedral $PbNb_2O_6$, which is not ferroelectric; ruling out piezoelectric properties and piezoelectric applications. So, most R & D efforts have been concentrated on orthorhombic $PbNb_2O_6$ [1–5, 12–21]. Even the real part (ε') and imaginary part (ε'') of the dielectric constant of the nonferroelectric $PbNb_2O_6$ with rhombohedral phase have rarely been reported [16, 22]. No analysis of its dielectric data has yet been made to study paraelectric and other physical properties in detail, although rhombohedral $PbNb_2O_6$ is a dielectric material in its own right. So, an analysis of its dielectric data [23] has been carried out in this work, after preparing rhombohedral $PbNb_2O_6$ in practically pure state, with X-ray Rietveld confirmation of the structure and impedance spectroscopy (IS) covering 20 Hz to 5.5 MHz at different values the sample temperature (T) up to 700°C.

2. Materials and Methods

Pellets from starting chemicals of PbO and Nb_2O_5 with 2% extra by weight of PbO (to compensate for presumed Pb loss

during firing) have been calcined first for 3.5 h at 1050°C, then at 1290°C for 1 h, and finally at 1270°C for about 5 h. At the end of last firing, the samples have been slow-cooled at an average rate of 1.5°C per minute, to get the rhombohedral form. The samples have been characterized by XRD with Rietveld analysis [16]. Firing in compact pellet form and grinding plus repelletizing before each firing improved sample quality.

The impedance spectroscopy has been carried out using Solatron "SI 1260 Impedance Gain Phase Analyzer" with a high temperature attachment. Our slow-cooled PNS pellets (diameter ~12 mm and 2.2 to 2.4 mm thick) have not been poled before measurement. Silver paint put on the flat faces of the pellet under study has acted as the electrodes for IS measurements, using 100 mV AC excitation. This measurement of ε' and ε'' (the real and imaginary components, resp., of the relative dielectric constant, i.e., permittivity) has been done for different measuring frequencies covering from 20 Hz to 5.5 MHz range at different values the sample temperature (T) while heating at the rate of 2°C per minute from room temperature to 700°C and also during many of the cooling runs.

3. Results and Discussion

X-ray Rietveld analysis shown in Figure 1 confirmed the rhombohedral PN structure with detected but unidentified impurity phase or phases, at a concentration of the order of 1% only. Impurity content can definitely be concluded to be lower than 5%. Due to factors like the unaccounted contribution of the unidentified impurities, the fit gives residue factors R_p = 15.1% and R_{wp} = 19.7%, although it looks fairly good. Since this paper is finding the structure only to confirm the formation of rhombohedral PN and not trying to improve the well-established [22] structure of rhombohedral PN, somewhat poorer quality of fit can be tolerated. Still, this fit does show the correct space group, R3 m (hexagonal), no. 160, with lattice parameters $a = b = 10.473(2)$ Å and $c = 11.536(2)$ Å. From the cell volume defined by these lattice parameters and formula-guided mass associated with the cell, density has been calculated to be about 83.8% of the theoretical density on average. This lower than 100% density can affect the measurement of dielectric properties only to the extent of showing a lower value of dielectric constant.

Figure 2 shows temperature (T) dependence of the real part of the dielectric constant (ε') during heating from room temperature to 700°C, at various measurement frequencies (5.5 MHz, 5 MHz, 4 MHz, 3 MHz, 2 MHz, 1 MHz, 500 kHz, 50 kHz, 30 kHz, 10 kHz, 5 kHz, and 1 kHz) for the rhombohedral phase. Two insets offer enlarged view in the temperature range from 400°C to 700°C. There appear to be two broad but weak peaks T_{peak1} (at 479°C to 509°C) and T_{peak2} (at 571°C to 575°C) for different lower frequency (5 kHz to 50 kHz) results and only one broad but weak peak T_{peak2} (at 572°C to 577°C) for higher frequencies (500 kHz to 5.5 MHz). Even a third peak appears at the lowest measuring frequency of 1 kHz. This T_{peak3} peak (at ~684°C) is rather sharp. This T_{peak2} matches, with respect to temperature, the ferroelectric to paraelectric transition [16] of orthorhombic $PbNb_2O_6$,

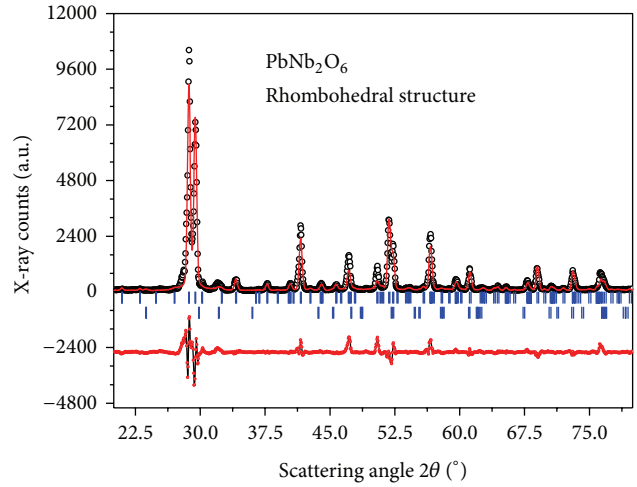

Figure 1: XRD pattern of the slow-cooled $PbNb_2O_6$ sample (as symbols), Rietveld-refined fit (red line), and the difference. The starting parameters were from [22]. More in the text.

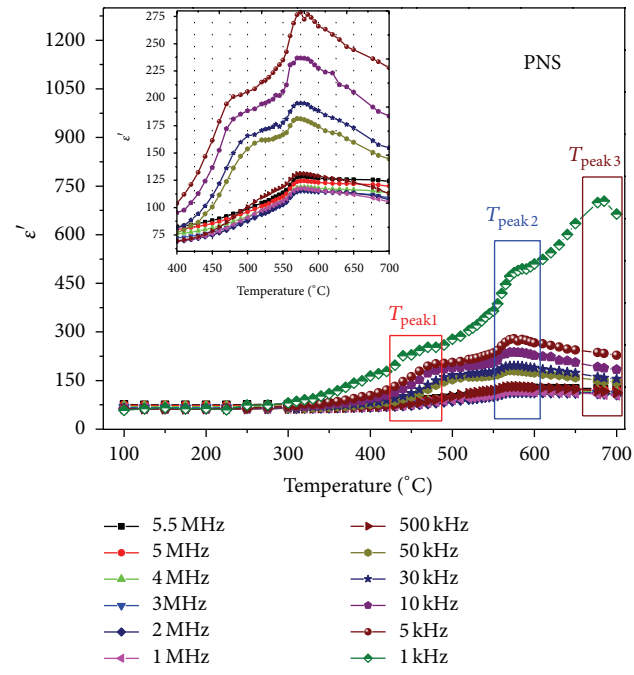

Figure 2: Temperature (T) dependence of the real part of the dielectric constant (ε') during heating runs at various frequencies (5.5 MHz, 5 MHz, 4 MHz, 3 MHz, 2 MHz, 1 MHz, 500 kHz, 50 kHz, 30 kHz, 10 kHz, 5 kHz, and 1 kHz) for the rhombohedral phase of $PbNb_2O_6$. Inset enlarges 400°C to 700°C view of the ε' versus T graph. After 700°C cycling in Figure 4, presently observed low intensity peaks, marked in the present figure, got removed.

confirming its presence as an impurity of much lower value of ε_{peak2} (height at peak2), compared to the value of ε_{max} [16] of the ferroelectric $PbNb_2O_6$, as detailed in Table 1, implying presence in low concentration. While the origin of other peaks or even of the ε_{peak2} peak is not very clear, their absence (Figure 4) in cooling runs confirms their origin to

Table 1: Values, for paraelectric $PbNb_2O_6$ (rhombohedral $PbNb_2O_6$), of ε' and $\tan\delta$ at room temperature and values of ε'_{peak1}, ε'_{peak2}, and ε'_{peak3} with the corresponding temperatures T_{peak1}, T_{peak2}, and T_{peak3}, as read from the experimental data during heating.

Frequency (Hz)	ε' (room temperature)	$\tan\delta$ (room temperature)	ε'_{peak1}	T_{peak1} (°C)	ε'_{peak2}	T_{peak2} (°C)	ε'_{peak3}	T_{peak3} (°C)
1 k	64.3	0.044	253.4	471.1 ± 3	495.8	584.4 ± 2	711.4	684.4 ± 2
5 k	64.0	0.013	204.0	479.5 ± 4	281.0	571.3 ± 3		
10 k	63.9	0.005	186.5	487.6 ± 5	238.8	574.9 ± 3		
30 k	63.8	0.003	165.6	497.6 ± 5	195.9	574.9 ± 3		
50 k	63.8	0.006	160.9	509.2 ± 6	182.0	573.3 ± 4		
500 k	64.1	0.051			131.3	572.8 ± 4		
1 M	64.9	0.106			117.8	575.5 ± 4		
2 M	65.1	−0.004			115.9	577.0 ± 5		
3 M	68.0	−0.004			115.2	577.0 ± 5		
4 M	71.7	0.002			118.7	575.9 ± 5		
5 M	75.3	−0.005			124.4	574.5 ± 5		
5.5 M	77.6	−0.026			128.5	575.5 ± 5		

Table 2: Real part of dielectric constant (ε') and dielectric loss ($\tan\delta$) of $PbNb_2O_6$ in rhombohedral phase, PNS sample, for different frequencies at two different temperatures for heating and cooling graphs. Here, ε'_{410} and ε'_{575} indicate the real part of dielectric constant at temperature 410°C and 575°C, respectively, and $\tan\delta_{410}$ and $\tan\delta_{575}$ indicate the dielectric loss values at 410°C and 575°C, respectively.

Frequency (Hz)	Heating run				Cooling run			
	ε'_{410}	$\tan\delta_{410}$	ε'_{575}	$\tan\delta_{575}$	ε'_{410}	$\tan\delta_{410}$	ε'_{575}	$\tan\delta_{575}$
1 k	171.3	2.839	483.0	120.0	13.89	−0.003	16.80	0.215
5 k	112.1	1.123	278.7	41.80	14.41	0.024	15.74	0.074
10 k	97.7	0.745	236.8	24.71	14.17	−0.028	15.61	0.043
30 k	83.6	0.394	195.5	10.11	14.20	−0.003	15.07	0.036
50 k	79.6	0.287	181.3	6.616	14.26	0.006	15.04	0.038
500 k	70.5	0.125	131.2	1.181	14.24	0.047	14.32	0.072
1 M	70.1	0.157	117.5	0.862	14.32	0.103	14.36	0.114
2 M	70.0	0.036	115.6	0.477	13.72	−0.029	13.66	−0.025
3 M	72.9	0.021	115.3	0.383	14.34	−0.105	14.35	−0.102
4 M	76.9	0.024	118.8	0.342	14.36	−0.117	14.35	−0.116
5 M	80.8	0.012	124.3	0.313	12.64	−0.276	12.65	−0.270
5.5 M	83.4	−0.016	128.4	0.290	11.68	−0.562	11.52	−0.558

low concentration unstable phases or defect conditions that get annealed by the 700°C cycling. Further discussion can found in the section on Cooling Data.

Figure 3 shows temperature dependence of the imaginary part of the dielectric constant (ε''), during heating from room temperature to 700°C for different measuring frequencies in the range 1 kHz to 5.5 MHz for PNS. For 1 kHz graph, ε'' increases sharply in the temperature range of 450°C to 650°C and then decreases with the increase of temperature, in our study being up to 700°C. Inset shows ε'' to be practically constant with temperature up to 450°C at high frequencies (1 MHz to 5.5 MHz). But for low frequencies (1 kHz to 500 kHz) and temperatures above 300°C, ε'' increases significantly with temperature. Cooling data (Figure 4), taken after cycling to 700°C, shows the temperature (T) dependence of the real part of dielectric constant (ε') as Figure 4(a). Inset Figures 4(b) and 4(c) show the temperature dependence of imaginary parts of dielectric constant (ε'') and temperature dependence of the dielectric loss ($\tan\delta$) at various measurement frequencies (5.5 MHz, 5 MHz, 4 MHz, 3 MHz, 2 MHz, 1 MHz, 500 kHz, 50 kHz, 30 kHz, 10 kHz, 5 kHz, and 1 kHz) during cooling (about 2°C/min) from 700°C to 410°C. Here, scale of plotting is grossly different from that for earlier heating data. We observe negative values of ε'' and $\tan\delta$ at high frequencies (5.5 MHz, 5 MHz, 4 MHz, 3 MHz, and 2 MHz). The values of ε', ε'', and $\tan\delta$ of PNS sample are much smaller and less affected by temperature in cooling runs than in heating runs, as has been shown in Table 2, as well. The nonconclusive jitter in data for 1 kHz may be due to the enlarged view of the signal, and hence not significant. It is clear that the 700°C cycling has removed the unstable phases or conditions (Figure 2) and provided a clearer view of the rhombohedral phase. Figure 5 shows frequency dependence of the real part (ε') of dielectric constant and $\tan\delta$ (inset view) of the PNS sample. In these heating runs at different temperatures (Figure 5),

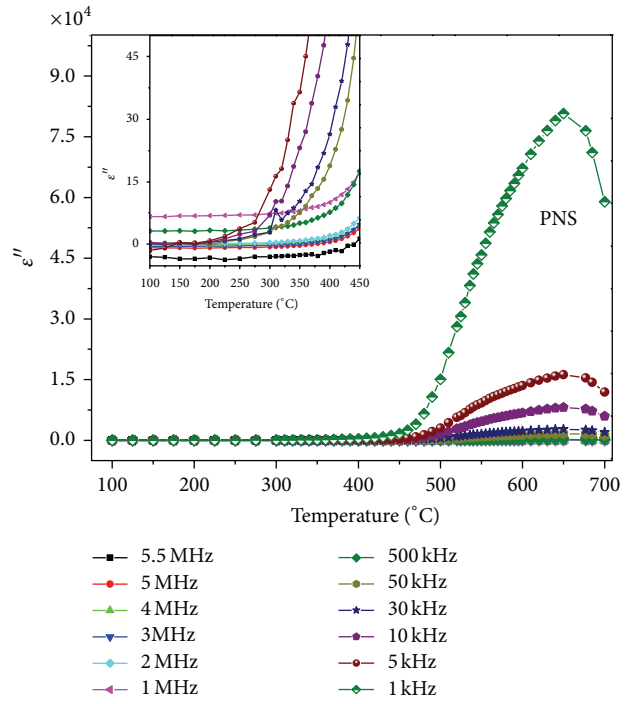

Figure 3: Temperature dependence of the imaginary part of the dielectric constant (ε'') during heating runs for different measuring frequencies in the range 1 kHz to 5.5 MHz for the paraelectric $PbNb_2O_6$. The inset shows details.

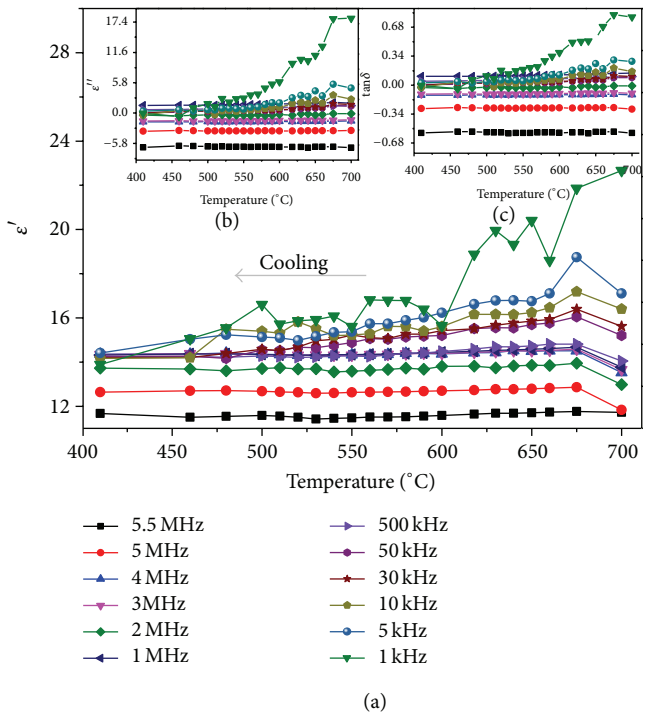

Figure 4: Cooling data for the rhombohedral phase of $PbNb_2O_6$, from 700°C to 410°C: (a) temperature dependence of the real part of dielectric constant (ε'), inset (b) temperature dependence of the imaginary part of dielectric constant (ε''), and (c) temperature dependence of the dielectric loss ($\tan\delta$), at various frequencies (1 kHz to 5.5 MHz).

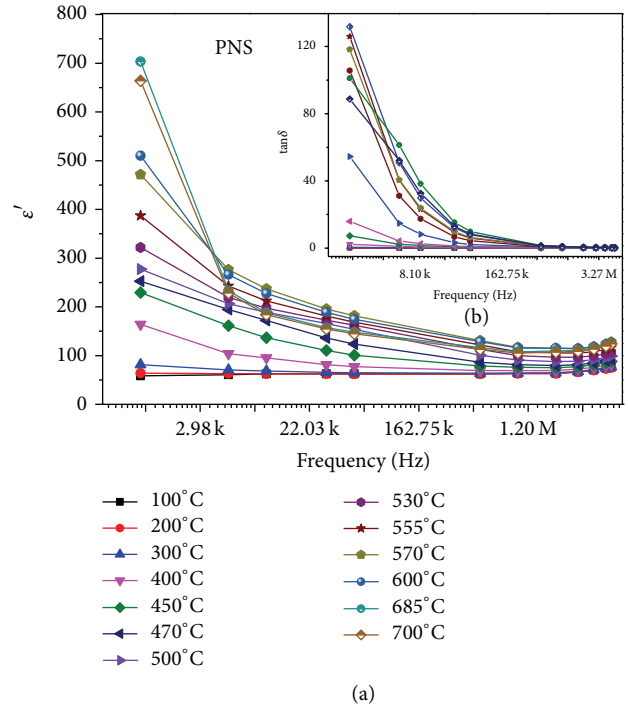

Figure 5: Frequency dependence of the real part (ε') of dielectric constant in the frequency range 1 kHz to 5.5 MHz, compiled from heating runs at different temperatures, for the rhombohedral phase of $PbNb_2O_6$. The inset is the variation of $\tan\delta$ in the same frequency and temperature range.

both quantities (ε' and $\tan\delta$) decrease with the increase of the measuring frequency.

In this section, proper analysis the dielectric data of rhombohedral $PbNb_2O_6$ (PNS samples) has been carried out to calculate the values of temperature has dependent relaxation time ($\tau = CR$), bulk resistance (R), and capacitance (C) using Nyquist diagram/Cole-Cole plot as well as frequency dependent AC conductivity (σ_{ac}) and frequency independent DC conductivity (σ_{dc}) for different temperatures. We also calculate the value of corresponding activation energy (E_a) for different temperature ranges.

The plot of Z'' (imaginary part of the impedance) versus Z' (real part of the impedance) is called Nyquist diagram [23]. It is based on the well-known Cole-Cole plot of ε'' versus ε'. The Z'' versus Z' plot for our rhombohedral PNS sample is shown in Figure 6. The data points have been joined by a standard polynomial fit, indicated by open circles in Figure 6. Single semicircular nature of the plots is clearer in the higher temperature plots (for 450°C to 700°C), as the lower temperature plots, like that for 400°C in the insert of Figure 6, show large semicircular arcs. An important observation is that the Nyquist diagram here shows only one semicircular arc [9, 23] in higher temperature region over the studied frequency range 20 Hz to 5.5 MHz. One semicircle implies only one contribution (here from the sample grains) and not from any second source like grain boundaries or electrode effect). A sample with one semicircle Nyquist diagram or Cole-Cole plot is equivalent [9, 23] to a bulk resistance R

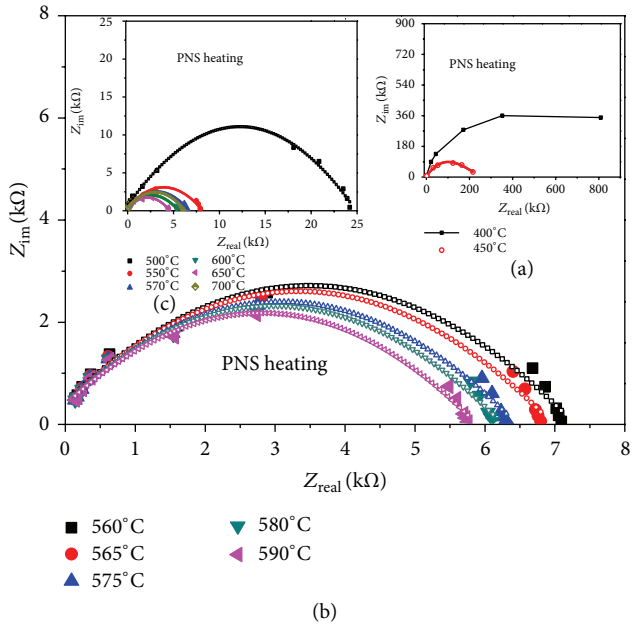

FIGURE 6: Plot of the imaginary part, Z_{im} in kΩ, of impedance versus its real part, Z_{real} in kΩ, for the paraelectric $PbNb_2O_6$ with rhombohedral phase, at temperatures (a) 400°C and 450°C (inset) (b) 560°C, 565°C, 580°C, and 590°C, and (c) 500°C, 550°C, 570°C, 600°C, 650°C, and 700°C (inset), since the complex impedance $Z^* = Z_{real} + jZ_{im}$, quantity $(-Z_{im})$ has actually been plotted in the figure.

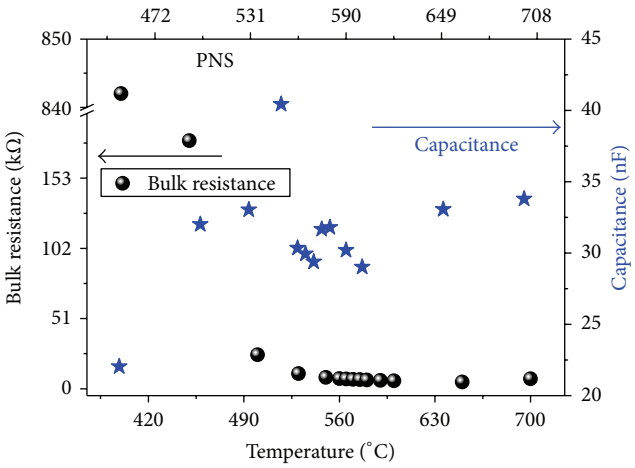

FIGURE 7: Bulk resistance R in $k\Omega$ (in left side, black solid sphere) and capacitance C in nF (in right side, blue solid star) of the equivalent RC circuit of slow cooled $PbNb_2O_6$ with rhombohedral phase, plotted against temperature, T. Here, R and C have been calculated from Nyquist diagram of Z' and Z'' in 20 Hz to 5.5 MHz range and the corresponding time constant $\tau = CR$, related to the dielectric relaxation time.

and a capacitance C in parallel. These elements give rise to a time constant $\tau = CR$, the dielectric relaxation time of the basic material. The frequency ω_m of the peak of the Nyquist diagram can find the relaxation time τ as $\omega_m \tau = 1$ for this peak point [9, 23]. At this point, Z'' has its maximum value. So, many authors use the frequency of peak (i.e., maximum) of Z'' versus frequency plot to find the relaxation time τ. Often the centre of the semicircular arc of the Nyquist diagram is not on the Z'-axis, so that the semicircle is seen to be depressed by an angle (θ) below the Z'-axis. This is the case, if there is a distribution of relaxation times. This θ is determined by the width of the distribution of relaxation time. Dielectric relaxation time (τ in μs) is a temperature-dependent parameter and it decreases with temperature, as has been shown in Figure 10.

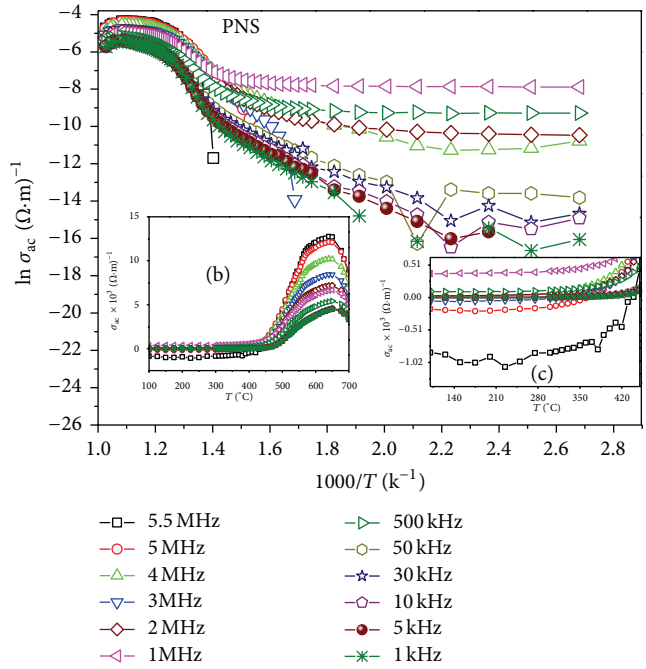

FIGURE 8: Frequency-dependent (a) AC conductivity ($\ln \sigma_{ac}$, σ_{ac} in $\Omega^{-1} \cdot m^{-1}$) as a function of $(1000/T$, in $K^{-1})$ over the temperature range 373 to 973 K (100 to 700°C) and insets (b) and (c) showing frequency-dependent AC conductivity as a function of T, in °C, in different temperature ranges for the rhombohedral $PbNb_2O_6$.

Further, if the semicircle starts near the origin at $Z' = R_\infty$ and intercepts the Z'-axis again at R_0, $R = (R_0 - R_\infty)$ gives [9, 23] the bulk resistance. Fitting the impedance spectroscopy (Z'' versus Z') data, usually forming an arch, to the equation of a circle, its radius r and θ and hence R_0 can be determined. Bulk resistance $R = (R_0 - R_\infty) = 2r \cdot \cos\theta$ has thus been calculated from our data in Figure 6 and plotted in Figure 7. It is found that the semicircle of data points for a particular temperature in Figure 6 reduces in size with increase of temperature, implying smaller bulk resistance of the sample at higher temperatures as documented in Figure 7 (left side, indicated by black solid sphere). Using the relation $\tau = CR$, we calculate the value of capacitance (C in nF) and plot in Figure 7 (right side, indicated by blue solid stars). In Figure 7, it is found that capacitance does not change much with temperature in region 500°C to 700°C except at the temperature ~550°C that gives a sharp peak.

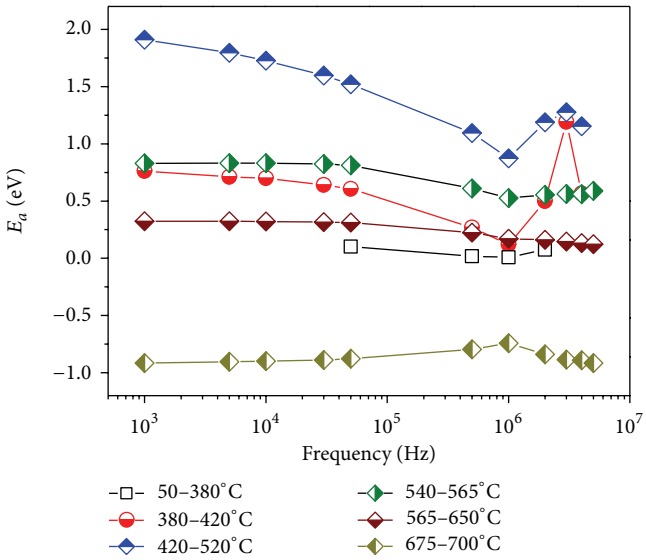

FIGURE 9: Frequency dependence of activation energy (E_{ac}) in different temperature ranges (50–380°C, 380–420°C, 420–520°C, 540–565°C, 565–655°C, and 675–700°C). Value of E_a calculated using the Arrhenius relation $\sigma_{ac} = \sigma_0 \exp(-E_{ac}/kT)$, where σ_0 is the pre-exponential factor, k is the Boltzmann constant that equals 8.617343×10^{-5} eV·K^{-1} and T is the temperature in Kelvin.

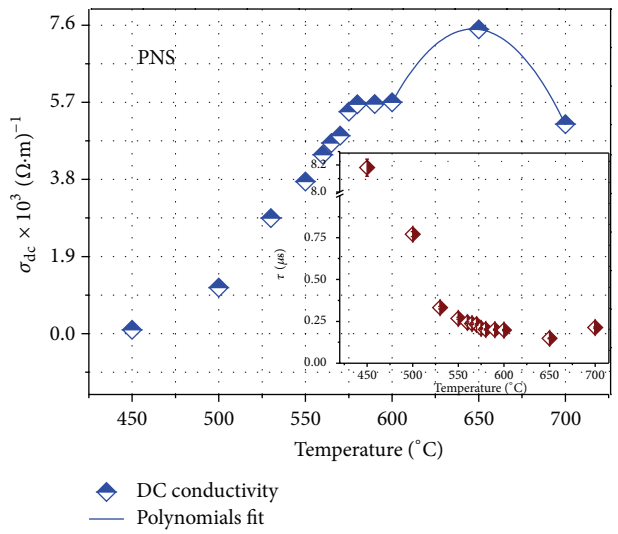

FIGURE 10: Temperature dependent DC conductivity (σ_{dc}) of the $PbNb_2O_6$ with rhombohedral phase, in the temperature range 400 to 700°C. Inset: temperature dependent relaxation time (τ, in μs) of the same sample in the same temperature range.

AC conductivity (σ_{ac}) has been calculated from the dielectric loss ($\tan\delta$) data using the empirical formula: $\sigma_{ac} = \omega\varepsilon_0\varepsilon' \tan\delta = 2\pi f\varepsilon_0\varepsilon''$ [9, 24], where $\varepsilon_0 = 10^7/4\pi c^2 = 8.854 \times 10^{-12}$ F·m^{-1} is the vacuum permittivity and c is the speed of light in vacuum. Figure 8(a) presents this result on AC conductivity (as σ_{ac}, in Ω^{-1}·m^{-1}) as a function of 1000/T (in Kelvin inverse, K^{-1}), inset Figure 8(b) shows σ_{ac} versus T in the temperature range 373 to 973 K (100 to 700°C), and Figure 8(c) shows σ_{ac} versus T in the temperature range 100 to 450°C. AC activation energy (E_{ac} in eV) has been calculated using the empirical Arrhenius relation $\sigma = \sigma_{ac} = \sigma_0 \exp(-E_{ac}/kT)$, where σ_0 is the preexponential factor, k is the Boltzmann constant (= 8.617343×10^{-5} eV·K^{-1}), and T is the temperature of the sample in Kelvin,and has listed the values of frequency-dependent E_{ac} in different temperature regions in Table 3, and variation of E_{ac} has been shown in Figure 9. Figure 9 shows the activation energy (E_{ac}) in frequency range 20 Hz to 50 kHz for different temperature ranges.

The frequency-independent and temperature-dependent DC conductivity (σ_{dc}) have been calculated using empirical formula [6, 25] $\sigma_{dc} = (\varepsilon_0\varepsilon_\infty)/\tau \cdot \sigma_{dc}$ for slow-cooled PN sample (paraelectric $PbNb_2O_6$) with rhombohedral structure, as shown in Figure 10. Here, we observe that the DC conductivity of the slow-cooled PN sample increases with temperature up to ~580°C, then remains practically constant up to 600°C, and then increases again giving a wide peak at 650°C. Data points have been joined by a continuous line through a polynomial fit of the equation $\sigma_{dc} = aT + bT^2$, where $a = 0.00107\ \Omega^{-1}$·m^{-1}·°C^{-1}, and $b = -8.27436 \times 10^{-7}\ \Omega^{-1}$·m^{-1}·°C^{-2}. Here, ε_0 (relative permittivity in vacuum) $= 8.854187 \times 10^{-12}$ F·m^{-1}, and ε_∞ is the real part of dielectric constant for high frequency. Here, τ is the time constant of the equivalent CR circuit (also called relaxation time), and this has been calculated using Nyquist diagram [9, 23] as detailed previously. Value of DC activation energy (E_{dc}), due to DC conductivity [9], has been calculated using the Arrhenius relation $\sigma_{dc} = \sigma_0 \exp(-E_{dc}/kT)$ [26], where σ_0 is the preexponential factor, k is the Boltzmann constant that equals 8.617343×10^{-5} eV·K^{-1}, and T is the temperature in Kelvin. The values of $E_{dc} = E_a$ and σ_0 have been summarized in Table 4.

Comparing the AC and DC conductivity data of PNS sample, we observe that $\sigma_{ac} < \sigma_{dc}$ (for frequencies from 1 MHz to 1 kHz) and $\sigma_{ac} > \sigma_{dc}$ (for frequencies 1 MHz to 5.5 MHz). Intriguing negative resistance can be noticed in Figures 8(b) and 8(c), although its confirmation by more experiments is desired. Negative resistance is, however, known in electronic devices and certain materials [27–30], and the granular ceramic PNS sample is a good candidate for such effects at high frequencies. This has indeed been observed here only at highest frequencies used. We plan to do further studies on this controversial issue.

Activation energy, calculated from DC conductivity, decreases with increase of temperature (Table 4). Negative activation energy for highest temperatures in Table 4 is linked to decrease of σ_{dc} with increase of temperature for $T \gtrsim 650$°C. However, negative values of DC and AC activation energy have been reported earlier [9, 31] without discussion. Presently observed AC activation energy is negative in the temperature range of 675–700°C, similar to positive and negative values of activation energy on two sides of a peak in [31] in their Figure 11 over 1 kHz to 1 MHz range studied there. This simply implies that thermal activation of carriers in a semiconductor, increases the resulting current with temperature up to a certain temperature. If no more carriers

Table 3: Calculated activation energy using the empirical formula $\sigma_{ac} = \sigma_0 \exp(-E_{ac}/kT) = 2\pi f \varepsilon_0 \varepsilon' \tan\delta = 2\pi f \varepsilon_0 \varepsilon''$, where E_{ac} is the activation energy, k is the 8.617343×10^{-5} eV·K^{-1}, and ε_0 is the 8.854187×10^{-12} F·m^{-1}. Values of E_{ac} and σ_0 for different measuring frequencies and temperatures ranges have been given in (a) 50 to 520°C and (b) 540 to 700°C.

(a)

Frequency (Hz)	Temperature range (50 to 380°C)		(380 to 420°C)		(420 to 520°C)	
	E_a (meV)	σ_0 $(\Omega\cdot m)^{-1} \times 10^5$	E_a (meV)	σ_0 $(\Omega\cdot m)^{-1} \times 10^6$	E_a (meV)	σ_0 $(\Omega\cdot m)^{-1} \times 10^{-6}$
1 k	—	—	766.7	119.8	1910.4	2223.8
5 k	—	—	715.1	64.9	1795.8	401.2
10 k	—	—	704.1	62.3	1727.0	144.7
30 k	—	—	644.2	29.2	1597.7	21.8
50 k	101.61	2.29	610.2	19.6	1519.4	7.26
500 k	17.96	15.37	272.5	0.239	1094.2	0.023
1 M	9.07	49.02	122.4	0.046	872.6	0.001
2 M	75.45	25.22	503.0	13.9	1188.5	0.145
3 M	—	—	1196.2	1.85 M	1276.0	0.642
4 M	—	—	570.4	63.3	1153.8	0.124

(b)

Frequency (Hz)	Temperature range (540 to 565°C)		(565 to 650°C)		(675 to 700°C)	
	E_a (meV)	σ_0 $(\Omega\cdot m)^{-1}$	E_a (meV)	σ_0 $(\Omega\cdot m)^{-1}$	E_a (meV)	σ_0 $(\Omega\cdot m)^{-1} \times 10^9$
1 k	829.6	303.6	324.0	0.273	−915.4	59.7
5 k	830.6	309.4	322.9	0.270	−904.2	68.9
10 k	830.6	310.5	320.9	0.264	−897.6	74.9
30 k	824.3	319.3	316.1	0.250	−889.3	83.6
50 k	813.0	248.3	311.6	0.238	−878.3	96.2
500 k	610.3	19.9	224.3	0.093	−795.3	308.5
1 M	525.4	7.84	171.2	0.059	−741.0	736.4
2 M	554.2	12.8	161.3	0.056	−839.9	233.6
3 M	561.8	17.0	145.7	0.054	−885.5	156.6
4 M	561.0	20.5	131.8	0.055	−890.9	176.2
5 M	588.0	35.6	123.3	0.059	−916.2	152.7

are available, further increase of temperature cannot lead to more carriers. But factors like scattering by increasing lattice vibration and recombination lead to decrease of current and hence of conductivity. Already energetic carriers lose energy in such processes. Application of activation equation to such cases gave negative activation energy.

4. Conclusion

Presently prepared $PbNb_2O_6$ samples have practically pure rhombohedral phase as revealed by X-ray diffraction. The samples are further characterized by impedance spectroscopy (IS) over 20 Hz to 5.5 MHz and up to 700°C. Cooling data of IS measurement appear to reveal better the real features of this paraelectric material; unexplained features (small broad peak/s in ε' versus T graph in Figure 2), appearing in the first heating run in IS measurement on our PNS sample, are conjectured to be related to minor phases at low concentration. 700°C cycling removes unexplained features, and no such unexplained peaks have been observed in the cooling data.

Present analysis of the impedance spectroscopy data on rhombohedral PNS has been very detailed over wide ranges of temperature and frequency, with DC and AC conductivities, capacitance (C), and resistance (R) of the equivalent CR circuit, relaxation time, and related activation energies evaluated and discussed either more extensively than the literature or for the first time. Here, we are the first to present the Nyquist diagram and the plot of Z_{im} versus Z_{real}, for rhombohedral lead meta-niobate. For the AC and DC conductivity of PNS sample we observe $\sigma_{ac} < \sigma_{dc}$ for frequencies in 1 MHz to 1 kHz range and $\sigma_{ac} > \sigma_{dc}$ for frequencies in 1 MHz to 5.5 MHz range. Rhombohedral $PbNb_2O_6$, frequently an undesirable impurity in orthorhombic $PbNb_2O_6$, is, however, a dielectric in its own right. The present work is its first detailed study from that viewpoint.

This pelletized sample appears to show negative resistance under certain conditions.

Table 4: Calculated activation energy in different temperature ranges, using the empirical formula $\sigma_{dc} = \sigma_0 \exp(-E_{dc}/kT) = \varepsilon_0\varepsilon_\infty/\tau$, where E_{dc} is the activation energy, $k = 8.617343 \times 10^{-5}$ eV·K^{-1} (Boltzmann constant), ε_0 (relative permittivity in vacuum) = 8.854187×10^{-12} F·m^{-1}, ε_∞ is the real part of dielectric constant for high frequency and τ is the time constant of the CR equivalent circuit, also called the relaxation time constant.

Temperature range (°C)	E_a (eV)	σ_0 $(\Omega\cdot m)^{-1}$
450–530	2.172	1.393×10^{11}
530–570	0.813	3.582×10^{2}
570–600	0.124	2.986×10^{-2}
650–700	−0.578	5.213×10^{-6}

Acknowledgments

The impedance spectroscopy setup at the Department of Ceramic Engineering, NIT, Rourkela 769008, India, has been used with the active encouragement of Professor Swadesh K Pratihar. Authors thank Professor Hamdy Doweidar for helpful comments.

References

[1] R. Kazys, A. Voleisis, and B. Voleisiene, "High temperature ultrasonic transducers: review," *Ultragarsas*, vol. 63, no. 2, pp. 7–17, 2008.

[2] R. A. Wolf and S. Trolier-McKinstry, "Temperature dependence of the piezoelectric response in lead zirconate titanate films," *Journal of Applied Physics*, vol. 95, no. 3, pp. 1397–1406, 2004.

[3] G. Goodman, "Ferroelectric properties of lead metaniobate," *Journal of the American Ceramic Society*, vol. 36, no. 11, pp. 368–372, 1953.

[4] M. H. Francombe and B. Lewis, "Structural, dielectric and optical properties of ferroelectric leadmetaniobate," *Acta Crystallographica*, vol. 11, pp. 696–703, 1958.

[5] E. C. Subbarao and G. Shirane, "Nonstoichiometry and ferroelectric properties of $PbNb_2O_6$-type compounds," *The Journal of Chemical Physics*, vol. 32, no. 6, pp. 1846–1851, 1960.

[6] X. Chen, H. Ma, W. Ding et al., "Microstructure, dielectric, and piezoelectric properties of $Pb_{0.92}Ba_{0.08}Nb_2O_6$-0.25 wt% TiO_2 ceramics: effect of sintering temperature," *Journal of the American Ceramic Society*, vol. 94, no. 10, pp. 3364–3372, 2011.

[7] G.-L. Men, P. Liu, R.-X. Zhang et al., "Effects of la on dielectric and piezoelectric properties of $Pb_{1-x}La_{2x/3}(Nb_{0.95}Ti_{0.0625})_2O_6$ ceramics," *Journal of the American Ceramic Society*, vol. 92, no. 8, pp. 1753–1757, 2009.

[8] X. M. Chen, X. G. Zhao, W. Ding, and P. Liu, "Microstructure and dielectric properties of $Pb_{0.94}La_{0.06}Nb_2O_6$ ceramics," *Ceramics International*, vol. 37, no. 7, pp. 2855–2859, 2011.

[9] K. R. Sahu and U. De, "Dielectric properties of $PbNb_2O_6$ up to 700°C from impedance spectroscopy," *Journal of Materials*, vol. 2013, Article ID 702946, 15 pages, 2013.

[10] K. R. Sahu and U. De, "Thermal characterization of piezoelectric and non-piezoelectric Lead Meta-Niobate," *Thermochimica Acta*, vol. 490, no. 1-2, pp. 75–77, 2009.

[11] U. De, K. R. Sahu, K. R. Chakraborty, and S. K. Pratihar, "Dielectric and thermal investigations on $PbNb_2O_6$ in pure piezoelectric phase and pure non-piezoelectric phase," *Integrated Ferroelectrics*, vol. 119, no. 1, pp. 96–109, 2010.

[12] S. Ray, E. Günther, and H.-J. Ritzhaupt-Kleissl, "Manufacturing and characterization of piezoceramic lead metaniobate $PbNb_2O_6$," *Journal of Materials Science*, vol. 35, no. 24, pp. 6221–6224, 2000.

[13] *Data sheet Fa. Ferroperm, Ferroperm A/S*, Piezoceramic Division, Kvistgard, Denmark, 1995.

[14] Y.-M. Li, L. Cheng, X.-Y. Gu, Y.-P. Zhang, and R.-H. Liao, "Piezoelectric and dielectric properties of $PbNb_2O_6$-based piezoelectric ceramics with high Curie temperature," *Journal of Materials Processing Technology*, vol. 197, no. 1–3, pp. 170–173, 2008.

[15] R. S. Rath, "Unit-cell data of the lead niobate $PbNb_20_6$," *Acta Crystallographica*, vol. 10, pp. 437–437, 1957.

[16] K. R. Chakraborty, K. R. Sahu, A. De, and U. De, "Structural characterization of orthorhombic and rhombohedral lead meta-niobate samples," *Integrated Ferroelectrics*, vol. 120, no. 1, pp. 102–113, 2010.

[17] F. Guerrero, Y. Leyet, M. Venet, J. de Los S. Guerra, and J. A. Eiras, "Dielectric behavior of the $PbNb_2O_6$ ferroelectric ceramic in the frequency range of 20 Hz to 2 GHz," *Journal of the European Ceramic Society*, vol. 27, no. 13-15, pp. 4041–4044, 2007.

[18] T. Lee and R. S. Lakes, "Damping properties of lead metaniobate," *IEEE Transactions on Ultrasonics, Ferroelectrics, and Frequency Control*, vol. 48, no. 1, pp. 48–52, 2001.

[19] S. G. Ingle and B. M. Bangre, "Optical, etching, and interferometric studies on ferroelectric $PbNb_2O_6$," *Pramana*, vol. 11, no. 4, pp. 435–440, 1978.

[20] W. N. Lawless, "Specific heats of lead and cadmium niobates at low temperatures," *Physical Review B*, vol. 19, no. 7, pp. 3755–3760, 1979.

[21] P. P. Labbe, M. Frey, B. Raveau, and J. C. Monier, "Structure Cristalline de la Phase Ferroelectrique du Niobate de Plomb $PbNb_2O_6$. Deplacements des Atomes Metalliques et Interpretation de la Surstructure," *Acta Crystallographica B*, vol. 33, pp. 2201–2212, 1977.

[22] R. Mahe, "Etude structurale du metaniobate de plomb rhomboedrique II. -Positions des atoms," *Bulletin de La Societe Chimique de France*, vol. 6, pp. 1879–1884, 1967.

[23] J. R. Macdonald and W. B. Johnson, "Impedance spectroscopy: theory, experiment, and applications," in *Fundamentals of Impedance Spectroscopy*, E. Barsoukov and J. R. Macdonald, Eds., pp. 1–26, John Wiley & Sons, Hoboken, NJ, USA, 2nd edition, 2005.

[24] R. N. P. Choudhary, D. K. Pradhan, G. E. Bonilla, and R. S. Katiyar, "Effect of La-substitution on structural and dielectric properties of $Bi(Sc_{1/2}Fe_{1/2})O_3$ ceramics," *Journal of Alloys and Compounds*, vol. 437, no. 1-2, pp. 220–224, 2007.

[25] Z. Lu, J. P. Bonnet, J. Ravez, and P. Hagenmuller, "Correlation between low frequency dielectric dispersion (LFDD) and

impedance relaxation in ferroelectric ceramic $Pb_2KNb_4TaO_{15}$," *Solid State Ionics*, vol. 57, no. 3-4, pp. 235–244, 1992.

[26] S. Indris, P. Heitjans, M. Ulrich, and A. Bunde, "AC and DC conductivity in nano- and microcrystalline Li_2O:B_2O_3 composites: experimental results and theoretical models," *Zeitschrift für Physikalische Chemie*, vol. 219, no. 1, pp. 89–103, 2005.

[27] S. M. Sze, *Physics of Semiconductor Devices*, Wiley-India, New Delhi, India, 2nd edition, 2007.

[28] J. Millman and C. C. Halkias, *Integrated Electronics: Analog to Digital Circuits and Systems*, chapter 3, Tata McGraw-Hill, New York, NY, USA, 1991.

[29] D. Dascălu, "Space-charge waves and high-frequency negative resistance of SCL diodes," *Electronics*, vol. 25, no. 4, pp. 301–329, 1968.

[30] S. Wang and D. D. L. Chung, "Apparent negative electrical resistance in carbon fiber composites," *Composites Part B*, vol. 30, no. 6, pp. 579–590, 1999.

[31] K. N. Singh and P. K. Bajpai, "Dielectric relaxation in pure columbite phase of $SrNb_2O_6$ ceramic material: impedance analysis," *World Journal of Condensed Matter Physics*, vol. 1, pp. 37–48, 2011.